Progress In Electromagnetics Research, PIER 102, 81–93, 2010

BAND GAP EXTENSION IN A ONE-DIMENSIONAL TERNARY METAL-DIELECTRIC PHOTONIC CRYSTAL

C.-J. Wu, Y.-H. Chung, and B.-J. Syu

Institute of Electro-Optical Science and Technology
National Taiwan Normal University
Taipei 116, Taiwan

T.-J. Yang

Department of Electrical Engineering
Chung-Hua University
Hsinchu 300, Taiwan

Abstract—Comparing with an all-dielectric binary photonic crystal, we show, in this work, that the photonic band gap in ternary metal-dielectric photonic crystal can be significantly enlarged. First, the band gap enlargement due to the addition of the metallic film is examined in the case of normal incidence. Next, in the oblique incidence, a wider omnidirectional band gap can be obtained in such a ternary metal-dielectric photonic crystal. All the theoretical analyses are made based on the transfer matrix method together with the Drude model of metals.

1. INTRODUCTION

A photonic crystal (PC) is an artificial medium with a periodic structure stacked by alternating two different materials with distinct refractive indices. An all-dielectric PC is the most common one since its constituents are all dielectric materials and thus is referred to as a dielectric-dielectric PC (DDPC). A simple one-dimensional DDPC also known as a distributed Bragg reflector (DBR) plays an important role in modern photonics because of its wide use in solid-state lasers [1–3]. The existence of photonic band gap (PBG) in a PC prohibits the wave propagation when the wave frequency falls within the PBG. The PBG media have emerged as new optical materials in the optical and physical

Corresponding author: C.-J. Wu (jasperwu@ntnu.edu.tw).

communities, triggering a flood of researches in both the fundamental and applicational issues in the past two decades [4–10].

For a one-dimensional DDPC, a wide PBG is of necessity for the purpose of photonic applications. The PBG can be enlarged by several methods. For example, it can be widened by increasing the refractive index contrast in the constituent materials in a typical DBR [11]. Using a chirped or disordered PC, it is also achievable to enhance the PBG [12–17]. The PBG can also be further significantly widened in a heterostructured PC [18–20].

The above methods of making a wider PBG are mostly based on the binary DDPC, that is, a PC has two different materials in each period. In addition to the binary PC, a ternary PC is also a possible design to obtain the enlarged PBG [21]. A ternary PC means that there are three constituent materials in each period. There have been several reports on the ternary PCs. A one-dimensional ternary DDPC has been used to design a tunable optical filter [22] and, an optical sensing device [23, 24]. More recently, a ternary PC has been extended to include a plasma layer [25].

In addition to the DDPCs, the one-dimensional binary metal-dielectric photonic crystals (MDPCs) are of great interest. Using ultrathin metallic films in the MDPCs, a variety of filtering responses and high-Q cavities are obtainable [26, 27]. Studies of photonic band structures in binary MDPCs are also available [28, 29]. It is also shown the PBG of a binary DDPC can be enhanced with the addition of metallic silver [17].

In this paper, the PBG in a ternary metal-dielectric photonic crystal (MDPC) is theoretically examined. It is found that the PBG can be enhanced pronouncedly with the inclusion of metal layer compared to the usual binary DDPC. We first investigate the band gap enlargement in the normal incidence case. The PBG enhancement due to different thicknesses of the metallic layer will be illustrated. Next, we shall investigate the onmidirectional PBG in the case of oblique incidence. The results illustrate that there exists a significant enhancement in the onmidirectional PBG, as compared to the usual binary DDPC.

2. BASIC EQUATIONS

The one-dimensional ternary MDPC is modeled as an N-period periodic multilayer immersed in air ($n_0 = 1$) shown in Fig. 1, in which the metallic layer 2 is sandwiched by two dielectric layers 1 and 3 in each period. The thicknesses of the constituent layers are denoted by d_1, d_2, and d_3, respectively, and thus the spatial periodicity is

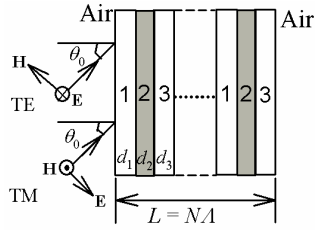

Figure 1. A model schematic of a one-dimensional ternary metal-dielectric photonic crystal, where, in each period, the metallic layer 2 is sandwiched by two dielectric layers 1 and 3. The total length $L = N\Lambda$, where the periodicity is $\Lambda = d_1 + d_2 + d_3$, and N is number of periods. The TE and TM waves are shown, respectively.

$\Lambda = d_1 + d_2 + d_3$. The total length of the system is $L = N\Lambda$, where N is the number of periods. The electromagnetic responses for the dielectric layers 1 and 3 are described by their indices of refraction n_1 and n_3, respectively. As for the metal layer, the usual Drude model will be employed. The temporal part of any field is assumed to be $e^{-j\omega t}$. Then the permittivity of the metal in Drude model takes the form

$$\varepsilon_2(\omega) = 1 - \frac{\omega_p^2}{\omega^2 + j\gamma\omega}, \tag{1}$$

where ω_p is the plasma frequency and γ is the damping frequency. The index of refraction of a metal is thus given by $n_2 = \sqrt{\varepsilon_2}$.

The photonic band gap of a PC can be viewed in terms of the calculated high-reflectance range (HRR) in the reflectance spectrum. For an electromagnetic wave incident obliquely on the most left boundary of air/layer1 at an angle of incidence θ_0, the reflectance can then be calculated by making use of the Abeles theory [30]. According to the Abeles theory, the characteristic matrix $M(\Lambda)$ for a single period must be determined first. The matrix is also dependent on the polarization of the incident wave. For the TE wave, $M(\Lambda)$ is expressed as

$$M(\Lambda) = \begin{bmatrix} M_{11} & M_{12} \\ M_{21} & M_{22} \end{bmatrix} = \prod_{\ell=1}^{3} \begin{bmatrix} \cos\beta_\ell & \frac{1}{jp_\ell}\sin\beta_\ell \\ -jp_\ell \sin\beta_\ell & \cos\beta_\ell \end{bmatrix}. \tag{2}$$

The matrix elements can be further calculated as follows [21, 22]:

$$\begin{aligned} M_{11} &= \cos\beta_1\cos\beta_2\cos\beta_3 - \frac{p_2}{p_1}\sin\beta_1\sin\beta_2\cos\beta_3 \\ &\quad -\frac{p_3}{p_2}\cos\beta_1\sin\beta_2\sin\beta_3 - \frac{p_3}{p_1}\sin\beta_1\cos\beta_2\sin\beta_3, \end{aligned} \tag{3a}$$

$$M_{12} = \frac{1}{jp_1}\sin\beta_1\cos\beta_2\cos\beta_3 + \frac{1}{jp_2}\cos\beta_1\sin\beta_2\cos\beta_3 + \frac{1}{jp_3}\cos\beta_1\cos\beta_2\sin\beta_3 - \frac{p_2}{jp_1p_3}\sin\beta_1\sin\beta_2\sin\beta_3, \quad (3b)$$

$$M_{21} = -jp_1\sin\beta_1\cos\beta_2\cos\beta_3 - jp_2\cos\beta_1\sin\beta_2\cos\beta_3 - jp_3\cos\beta_1\cos\beta_2\sin\beta_3 + j\frac{p_1p_3}{p_2}\sin\beta_1\sin\beta_2\sin\beta_3, \quad (3c)$$

$$M_{22} = \cos\beta_1\cos\beta_2\cos\beta_3 - \frac{p_1}{p_2}\sin\beta_1\sin\beta_2\cos\beta_3 - \frac{p_2}{p_3}\cos\beta_1\sin\beta_2\sin\beta_3 - \frac{p_1}{p_3}\sin\beta_1\cos\beta_2\sin\beta_3. \quad (3d)$$

Here $\beta_\ell = k_0 n_\ell d_\ell \cos\theta_\ell$ and $p_\ell = n_\ell \cos\theta_\ell$, where $\ell = 1, 2$, and 3, respectively, $k_0 = \omega\sqrt{\mu_0\varepsilon_0}$ is the free-space wave number, and θ_ℓ is the corresponding ray angle determined by the Snell's law of refraction. It should be noted that the matrix elements are closely related to the photonic band structure for a ternary PC. In fact, based on the Bloch theorem and translational symmetry, the half trace $(M_{11} + M_{22})/2$ can be used to calculate the Bloch wave vector as a function of the frequency [11].

Next, the total characteristic matrix of the entire system is given by

$$M_T(N\Lambda) \equiv \begin{bmatrix} m_{11} & m_{12} \\ m_{21} & m_{22} \end{bmatrix} = [M(\Lambda)]^N = \begin{bmatrix} M_{11} & M_{12} \\ M_{21} & M_{22} \end{bmatrix}^N, \quad (4)$$

where the matrix elements of M_T can be obtained in terms of the elements of the single-period matrix, namely

$$m_{11} = M_{11}U_{N-1}(a) - U_{N-2}(a), \quad (5a)$$

$$m_{12} = M_{12}U_{N-1}(a), \quad (5b)$$

$$m_{21} = M_{21}U_{N-1}(a), \quad (5c)$$

$$m_{22} = M_{22}U_{N-1}(a) - U_{N-2}(a), \quad (5d)$$

where U_N is the Chebyshev polynomial of the second kind given by

$$U_N(a) = \frac{\sin\left[(N+1)\cos^{-1}a\right]}{\sqrt{1-a^2}}, \quad (6)$$

where the argument a is the half trace of the single-period matrix, i.e.,

$$a = \frac{1}{2}(M_{11}+M_{22}) = \cos\beta_1\cos\beta_2\cos\beta_3 - \frac{1}{2}\left(\frac{p_1}{p_2}+\frac{p_2}{p_1}\right)\sin\beta_1\sin\beta_2\cos\beta_3 - \frac{1}{2}\left(\frac{p_2}{p_3}+\frac{p_3}{p_2}\right)\cos\beta_1\sin\beta_2\sin\beta_3 - \frac{1}{2}\left(\frac{p_1}{p_3}+\frac{p_3}{p_1}\right)\sin\beta_1\cos\beta_2\sin\beta_3. \quad (7)$$

Having obtained the matrix elements in Eq. (5), one can calculate the reflectance $R = r * r$, where the reflection coefficient r of the system is given by

$$r = \frac{(m_{11} + m_{12}p_0)\, p_0 - (m_{21} + m_{22}p_0)}{(m_{11} + m_{12}p_0)\, p_0 + (m_{21} + m_{22}p_0)}, \tag{8}$$

where $p_0 = n_0 \cos\theta_0$. The above formulations can also be applied for the TM wave by a simple replacement of $p_\ell = \cos\theta_\ell / n_\ell$, where $\ell = 0, 1, 2$, and 3, respectively.

3. NUMERICAL RESULTS AND DISCUSSION

In the next calculation, the layers 1 and 3 are taken to be ZnSe and Na_3AlF_6 whose refractive indices and thicknesses are $n_1 = 2.6$ [3], $d_1 = 90\,\text{nm}$ and $n_3 = 1.34$ [3], $d_3 = 90\,\text{nm}$, respectively. The exciton effects in semiconducting layer 1, ZnSe, are neglected [31] because exciton absorption is important in the discussion of optical properties in the ultraviolet region, which is beyond the region of interest in this work. The metallic layer is taken to be silver (Ag) with the plasma frequency $\omega_p = 2\pi \times 2.175 \times 10^{15}\,\text{rad/s}$ [32], and the damping frequency is $\gamma = 2\pi \times 4.35 \times 10^{12}\,\text{rad/s}$ [32]. In what follows we shall numerically demonstrate the calculated wavelength-dependent reflectance $R\,(\lambda)$ at a fixed number of periods $N = 20$.

3.1. Normal Incidence

In Fig. 2, we plot the reflectance spectrum for the usual binary DDPC, that is, the metal layer 2 is absent in structure shown in Fig. 1. It is seen that there exists a PBG or HRR with a bandwidth of 270 nm because its left and right band edges are $\lambda_L = 605\,\text{nm}$ and $\lambda_R = 875\,\text{nm}$. In

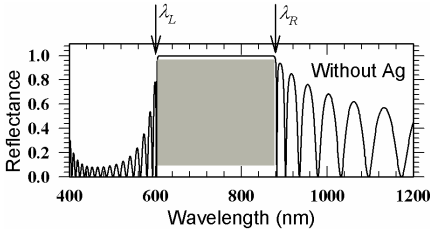

Figure 2. The calculated wavelength-dependent reflectance in the absence of the metal Ag. The HHR ranges from $\lambda_L = 605$ to $\lambda_R = 875\,\text{nm}$ with a bandwidth of $\Delta = \lambda_R - \lambda_L = 270\,\text{nm}$.

fact, these two band edges in a binary DDPC can be determined by the solutions from the following analytic equation [3],

$$\cos^2\left(\frac{\delta_1+\delta_3}{2}\right) = \rho^2\cos^2\left(\frac{\delta_1-\delta_3}{2}\right), \tag{9}$$

where $\delta_1 = 2\pi n_1 d_1/\lambda$, $\delta_3 = 2\pi n_3 d_3/\lambda$, and $\rho = (n_1 - n_3)/(n_1 + n_3)$ is the Fresnel coefficient. With the above material parameters, Eq. (9) leads to $\lambda_L = 605.4\,\text{nm}$ and $\lambda_R = 875.3\,\text{nm}$, in good agreement with those shown in Fig. 2.

When the metallic film Ag with a thickness of 10 nm is introduced to form a ternary MDPC shown in Fig. 1, the HRR shown in Fig. 3(a) is apparently enlarged [31], as compared to Fig. 2. The bandwidth is increased up to 320 nm. In addition, the HRR is totally shifted to the shorter wavelength because both λ_L and λ_R are moved to the shorter wavelength. The amount of shift in λ_L is more pronounced than that in λ_R. If the thickness of Ag is increased to $d_2 = 20\,\text{nm}$, the result is then shown in 3(b). The HRR continues to enhance as the metal thickness increases, as illustrated in 3(c) (with $d_2 = 30\,\text{nm}$) and 3(d) (with $d_2 = 50\,\text{nm}$). To take a close look at the dependence of band edges on the thickness, in Fig. 4, we now plot the band edges λ_L and λ_R as a function of d_2. The shaded region denotes the HRR, which

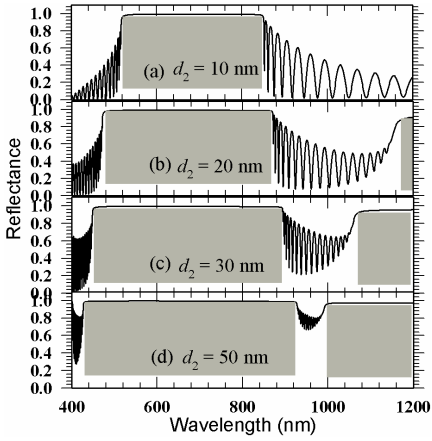

Figure 3. The calculated wavelength-dependent reflectance in a ternary MDPC with a metal Ag. In (a), the thickness is $d_2 = 10\,\text{nm}$ and the HHR ranges from 520–840 nm with bandwidth of 320 nm. In (b), $d_2 = 20\,\text{nm}$ and HRR is 480–875 nm with bandwidth of 395 nm. In (c), $d_2 = 30\,\text{nm}$ and (d), $d_2 = 50\,\text{nm}$, the HRR is significantly enlarged with the increase in the thickness of metal film.

increases with the increase in the metal thickness. While the left band edge λ_L monotonously decreases with increasing d_2, the right band edge λ_R first decreases at a thinner film of less than 10 nm and then increases with the increase in d_2. The wider HRR covers the visible and near infrared regions when d_2 is larger than 50 nm.

The physical origin of the band gap produced by the inclusion of the metal layer comes from the fact that the real part of permittivity in Eq. (1) is negative at frequency less than the plasma frequency. Thus wave propagation in a metal layer will be attenuated, meaning that the wave will be reflected. In a pure DDPC, the band gap comes from the Bragg reflection from the interfaces. The inclusion of metal layer causes the pass bands in DDPC to be suppressed. As a result, the band gap is increased. In addition, if the thickness of metal layer is increased, then the MDPC will reflect almost all waves like a purely metallic reflector.

In addition, in Figs. 3(b), (c), and (d), there is an additional low-frequency band gap. This gap may be useful to allow us to determine the effective plasma frequency for a ternary MDPC. In Ref. [29], the effective plasma frequency has been defined in a binary MDPC. The

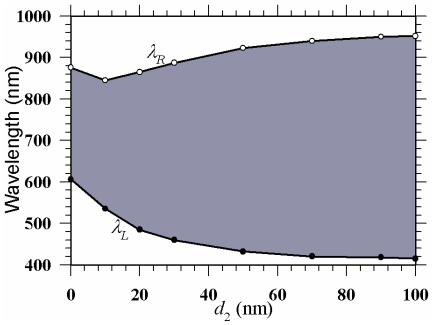

Figure 4. The calculated left and right band edges as a function of the metal thickness. It is seen that bandwidth of HRR, $\Delta = \lambda_R - \lambda_L$, increases as the metal thickness increases.

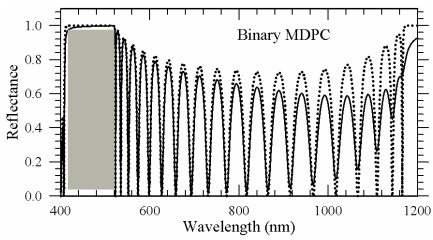

Figure 5. The calculated reflectance response for a binary MDPC of the structure is $Air/(M/D)^N/Air$. Here M is Ag and the index of D is taken to be 2.6. The HRR falls between 400 and 500 nm. The solid curve is for the inclusion of loss of $\gamma = 2\pi \times 4.35 \times 10^{12}$ rad/s, while the dotted curve is for the lossless case, i.e., $\gamma = 0$.

determination of the effective plasma frequency for a ternary MDPC will be of interest to us and we are going to investigate this issue.

Now let us make a brief comparison between the ternary MDPC and the binary MDPC. In Fig. 5, a narrow HRR between 400 and 500 nm is found for a binary MDPC (the solid curve), in which the dielectric layer D with a refractive index of 2.6 has been used. The thickness of Ag is 10 nm and 90 nm for D. Comparing with Figs. 5 and 3(a), it is seen again that the ternary MDPC has a wider HRR than the binary one.

In Fig. 5, we have also plotted the reflectance in the absence of the loss, i.e., $\gamma = 0$, as illustrated in the dotted curve. We see that the flat-top HRR around 400–500 nm is not changed substantially even the loss is incorporated. However, the sidelobes are strongly affected by the inclusion of loss. It is noted that the original flat-top near 1200 nm in the lossless case is strongly destroyed. The result indicates the effect of loss on the HRR is salient in the long wavelength regime. This can be seen from the Drude formula Eq. (1) which indicates that the role played by the loss parameter γ will emerge at low frequency or long wavelength. At shorter wavelength such as at 400–500 nm, the HRR is essentially not influenced since γ is not important there.

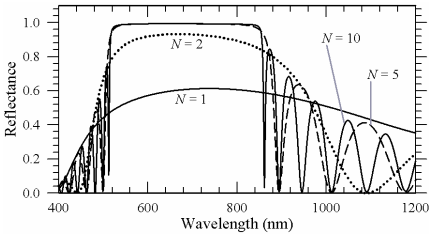

Figure 6. The calculated wavelength-dependent reflectance in a ternary MDPC with a metal Ag ($d_2 = 10$ nm) at different $N = 1, 2, 5$, and 10. The thickness $d_2 = d_3 = 90$ nm are used as in Fig. 3. The HRR is obtained at $N = 10$.

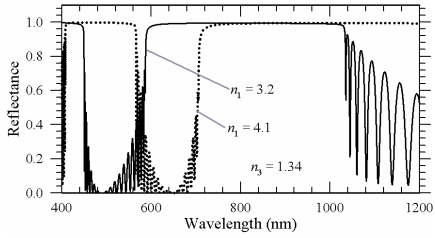

Figure 7. The calculated wavelength-dependent reflectance in a ternary MDPC with a metal Ag ($d_2 = 10$ nm) at different refractive-index contrast in dielectric layers 1 and 3. The thickness $d_2 = d_3 = 90$ nm are used as in Fig. 3.

Before we go on to the angle-dependent reflectance response, let us continue to investigate other factors such as the number of periods, N, the values in n_1 and n_3, and the plasma frequency of the metal. Fig. 6 displays the reflectance response for a ternary MDPC at different

values in N. The conditions of calculation are the same as those in Fig. 3(a). It is seen that the flat-top HRR can be reached as $N = 10$. Comparing with $N = 20$ in Fig. 3(a), we see that the very difference only appears in the sidelobes. That is, the value of N is at best to be taken at least 10 in order to obtain the HRR.

Figure 7 illustrates the reflectance response at different index contrasts in dielectric layers 1 and 3. The conditions in Fig. 3(a) are used here but the refractive index n1 is increased to 3.2 (solid curve) and 4.1 (dotted curve), respectively. Like in the binary PC, it is seen that the band gap in Fig. 3(a) can be enhanced due to the increase in the index contrast n_1/n_3 with n_3 being fixed. Moreover, the band gap is shifted to the long wavelength. With this shift, another band gap emerges near 400 nm. The band gap is strongly extended if n_1 is increases up to 4.1. The variation in the index contrast in the dielectric layers has thus two effects, that is, the extension and shift in the band gap. The typical features in a Bragg gap are thus illustrated in a ternary PC.

In Fig. 8, we show the effect of different plasma frequency on the reflectance response. Because different metal has a different plasma frequency, we have taken Cu, Ag and Al with $\omega_p = 2\pi \times 1.914 \times 10^{15}$, $2\pi \times 2.175 \times 10^{15}$, and $2\pi \times 3.570 \times 10^{15}$, respectively [31]. The metal with higher plasma frequency will move the band gap to the left, the shorter wavelength. In addition, the band gap is also increased.

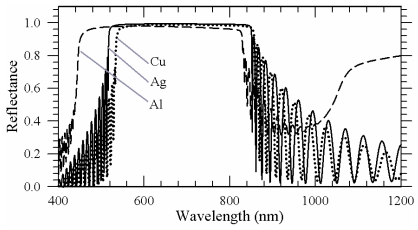

Figure 8. The calculated wavelength-dependent reflectance in a ternary MDPC with different metals Cu, Ag and Al with the same $d_2 = 10$ nm. The thickness $d_2 = d_3 = 90$ nm are used as in Fig. 3.

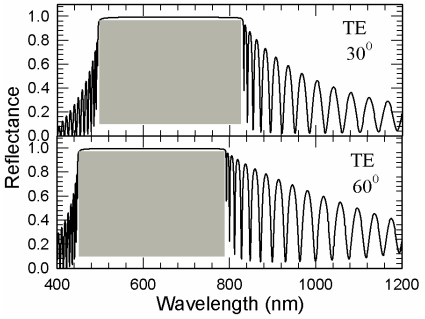

Figure 9. The calculated reflectance at two distinct incident angels of 30° and 60° for the TE wave. Here the thickness of metal layer $d_2 = 10$ nm is used.

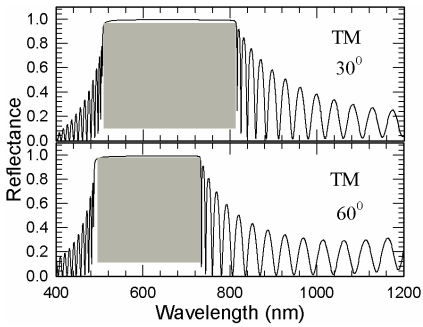

Figure 10. The calculated reflectance at two distinct incident angels of 30° and 60° for the TM wave. Here the thickness of metal layer $d_2 = 10\,\text{nm}$ is used.

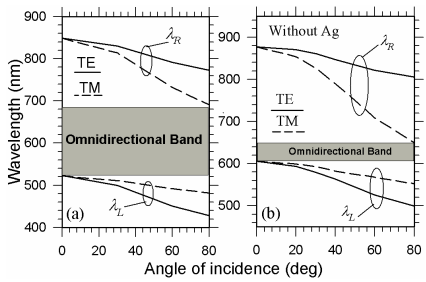

Figure 11. The calculated left and right band edges as a function of the angle of incidence for both TE and TM waves with a fixed metal thickness of $d_2 = 10\,\text{nm}$ (a) and without the metal Ag (b). The shaded region indicates the so-called omnidirectional band.

3.2. Oblique Incidence

In Fig. 9, we plot the reflectance response at two different angles of incidence at $d_2 = 10\,\text{nm}$ for the TE wave. The HRR is obviously enlarged when the angle of incidence increases, as compared to the normal-incidence HRR in Fig. 3(a). This trend of HRR in MDPC is also known in the usual DDPC [3]. As for the TM wave, the results shown in Fig. 10 demonstrate that the HRR will decrease as the angle increases. In addition, at the same angle of incidence, the HRR in TM wave is smaller than that of in TE wave. The whole results in Figs. 9 and 10 can be concluded in Fig. 11(a), in which the two angle-dependent band edges are plotted. The solid curve is for the TE wave, whereas the TM wave is the dash curve. It can be seen the omnidirectional HRR is found and locates from 520–680 nm, yielding an omnidirectional bandwidth of 360 nm.

Figure 11(b) depicts the band edges for the case of without Ag, i.e., $d_2 = 0$, that is, it reduces to the usual binary DDPC. It can be seen that the omnidirectional bandwidth for a PC with Ag is about four times larger than that without Ag. The results in Fig. 11 again demonstrate that the inclusion of metallic film in a ternary MDPC has a wider omnidirectional band. The role played by the metallic film in the enhancement of PBG is thus elucidated.

4. CONCLUSION

The photonic band structure in the visible and near infrared regions for a ternary MDPC has been theoretically investigated. It has been shown that the ternary MDPC has a superior feature in the enhancement of the HRR compared to the binary and ternary DDPC, and to the binary MDPC as well. In the normal incidence, the HRR can be significantly enlarged at a thicker metal film. In the oblique incidence, the existing omnidirectional band is obviously larger than that in the all-dielectric PC.

ACKNOWLEDGMENT

C.-J. Wu acknowledges the financial support from the National Science Council of the Republic of China (Taiwan) under Contract No. NSC-97-2112-M-003-013-MY3.

REFERENCES

1. Joannopoulos, J. D., R. D. Meade, and J. N. Winn, *Photonic Crystals: Molding the Flow of Light*, Princeton University Press, Princeton, NJ, 1995.
2. Sakoda, K., *Optical Properties of Photonic Crystals*, Springer-Verlag, Berlin, 2001.
3. Orfanidis, S. J., *Electromagnetic Waves and Antennas*, Rutger University, 2008, www.ece.rutgers.edu/ orfanidi/ewa.
4. Hsu, H.-T. and C.-J. Wu, "Design rules for a Fabry-Perot narrow band transmission filter containing a metamaterial negative-index defect," *Progress In Electromagnetics Research Letters*, Vol. 9, 101–107, 2009.
5. Srivastava, R., K. B. Thapa, S. Pati, and S. P. Ojha, "Omni-direction reflection in one dimensional photonic crystal," *Progress In Electromagnetics Research B*, Vol. 7, 133–143, 2008.
6. Banerjee, A., "Binary number sequence multilayer structure based on refractometric optical sensing element," *Journal of Electromagnetic Waves and Applications*, Vol. 22, No. 17–18, 2439–2449, 2008.
7. Wang, X., X. Hu, Y. Li, W. Jia, C. Xu, X. Liu, and J. Zi, "Enlargement of omnidirectional total reflection frequency range in one-dimensional photonic crystals by using photonic heterostructures," *Appl. Phys. Lett.*, Vol. 80, 4291–4293, 2002.
8. Fink, Y., J. N. Winn, S. Fan, C. Chen, J. Michel, J. D. Joannopou-

los, and L. E. Thomas, "A dielectric omnidirectional reflector," *Science*, Vol. 282, 1679–1682, 1998.

9. Yablonovitch, E., "Inhibited spontaneous emission in solid state physics and electronics," *Phys. Rev. Lett.*, Vol. 58, 2059-2062, 1987.
10. John, S., "Strong localization of photons in certain disordered lattices," *Phys. Rev. Lett.*, Vol. 58, 2486–2489, 1987.
11. Yeh, P., *Optical Waves in Layered Media*, John Wiley & Sons, Singapore, 1991.
12. Wu, C.-J., B.-H. Chu, M.-T. Weng, and H.-L. Lee, "Enhancement of bandwidth in a chirped quarter-wave dielectric mirror," *Journal of Electromagnetic Waves and Applications*, Vol. 23, No. 4, 437–447, 2009.
13. Wu, C.-J., B.-H. Chu, and M.-T. Weng, "Analysis of optical reflection in a chirped distributed Bragg reflector," *Journal of Electromagnetic Waves and Applications*, Vol. 23, No. 1, 129–138, 2009.
14. Wu, C.-J., Y.-N. Rao, and W.-H. Han, "Enhancement of photonic band gap in a disordered quarter-wave dielectric photonic crystal," *Progress In Electromagnetics Research*, PIER 100, 27–36, 2010.
15. Li, H., H. Chen, and X. Qiu, "Bandgap extension of disordered 1D binary photonic crystals," *Physica B*, Vol. 279, 164–167, 2000.
16. Tolmachev, V. A., T. S. Perova, J. A. Pilyugina, and R. A. Moore, "Experimental evidence of photonic band gap extension for disordered 1D photonic crystals based on Si," *Optics Comm.*, Vol. 259, 104–106, 2006.
17. Qi, L., Z. Yang, X. Gao, F. Lan, Z. Shi, and Z. Liang, "Bandgap extension of disordered one-dimensional metallic-dielectric photonic crystals," *IEEE International Vacuum Electronics Conference, IVEC*, 158–159, 2008.
18. Wang, X., X. Hu, Y. Li, W. Jia, C. Xu, X. Liu, and J. Zi, "Enlargement of omnidirectional total reflection frequency range in one-dimensional photonic crystals by using photonic heterostructures," *Appl. Phys. Lett.*, Vol. 80, No. 23, 4291–4293, 2002.
19. Zi, J., J. Wan, and C. Zhang, "Large frequency range of negligible transmission in one-dimensional photonic quantum well structures," *Appl. Phys. Lett.*, Vol. 73, No. 15, 2084–2086, 1998.
20. Srivastava, R., S. Pati, and S. P. Ojha, "Enhancement of omnidirectional reflection in photonic crystal heterostructures," *Progress In Electromagnetics Research B*, Vol. 1, 197–208, 2008.

21. Awasthi, S. K., U. Malaviya, and S. P. Ojha, "Enhancement of omnidirectional total-reflection wavelength range by using one-dimensional ternary photonic bandgap material," *J. Opt. Soc. Am. B: Optical Physics*, Vol. 23, 2566–2571, 2006.
22. Awasthi, S. K. and S. P. Ojha, "Design of a tunable optical filter by using a one-dimensional ternary photonic ban gap material," *Progress In Electromagnetics Research M*, Vol. 4, 117–132, 2008.
23. Banerjee, A., "Enhanced temperature sensing by using one-dimensional ternary photonic band gap structures," *Progress In Electromagnetics Research Letters*, Vol. 11, 129–137, 2009.
24. Banerjee, A., "Enhanced refractometric optical sensing by using one-dimensional ternary photonic crystals," *Progress In Electromagnetics Research*, PIER 89, 11–22, 2009.
25. Prasad, S., V. Singh, and A. K. Singh, "Modal propagation characteristics of EM waves in ternary one-dimensional photonic crystals," *Optik*, 2009.
26. Contopanagos, H., E. Yablonovitch, and N. G. Alexopoulous, "Electromagnetic properties of periodic multilayers of ultrathin metallic films from dc to ultraviolet frequencies," *J. Opt. Soc. Am. A*, Vol. 16, 2294–2306, 1999.
27. Contopanagos, H., N. G. Alexopoulous, and E. Yablonovitch, "High-Q radio-frequency structures using one-dimensionally periodic metallic films," *IEEE Trans. Microwave Theory Technol.*, Vol. 46, 1310–1312, 1998.
28. Keskinen, M. J., P. Loschialpo, D. Forester, and J. Schelleng, "Photonic band structure and transmissivity of frequency-dependent metallic-dielectric systems," *J. Appl. Phys.*, Vol. 88, 5785–5790, 2000.
29. Xu, X., Y. Xi, D. Han, X. Liu, J. Zi, and Z. Zhu, "Effective plasma frequency in one-dimensional metallic-dielectric photonic crystals," *Appl. Phys. Lett.*, Vol. 86, 091112, 2005.
30. Born, M. and E. Wolf, *Principles of Optics*, Cambridge, London, 1999.
31. Marquez-Islas, R., B. Flores-Desirena, and F. Pérez-Rodríguez, "Exciton polaritons in one-dimensional metal-semiconductor photonic crystal," *J. Nanosci. Nanotechnol.*, Vol. 8, 6584–6588, 2008.
32. Markos, P. and C. M. Soukoulis, *Wave Propagation: From Electrons to Photonic Crystals and Left-handed Materials*, Princeton University Press, New Jersey, 2008.